ACS OMEGA

http://pubs.acs.org/journal/acsodf

Article

Quinoidal Small Molecule Containing Ring-Extended Termini for Organic Field-Effect Transistors

Yoonjung Mok,[†] Yunseul Kim,[†] Yina Moon, Jong-Jin Park, Yeonsu Choi, and Dong-Yu Kim*

Cite This: *ACS Omega* 2021, 6, 27305−27314

Read Online

ACCESS | Metrics & More | Article Recommendations | Supporting Information

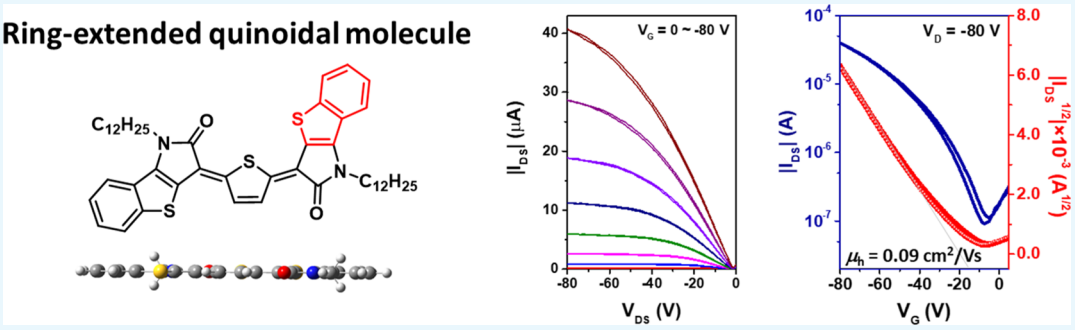

ABSTRACT: In this work, we synthesized and characterized two quinoidal small molecules based on benzothiophene modified and original isatin terminal units, benzothiophene quinoidal thiophene (BzTQuT) and quinoidal thiophene (QuT), respectively, to investigate the effect of introducing a fused ring into the termini of quinoidal molecules. Extending the terminal unit of the quinoidal molecule affected the extension of π-electron delocalization and decreased the bond length alternation, which led to the downshifting of the collective Raman band and dramatically lowering the band gap. Organic field-effect transistor (OFET) devices in neat BzTQuT films showed p-type transport behavior with low hole mobility, which was ascribed to the unsuitable film morphology for charge transport. By blending with an amorphous insulating polymer, polystyrene, and poly(2-vinylnaphthalene), an OFET based on a BzTQuT film annealed at 150 °C exhibited improved mobility up to 0.09 cm^2 V^{-1} s^{-1}. This work successfully demonstrated that the extension of terminal groups into the quinoidal structure should be an effective strategy for constructing narrow band gap and high charge transporting organic semiconductors.

1. INTRODUCTION

Organic semiconductors have attracted much attention in the academic and industrial fields owing to their potential applications in solution processability, lightweight and large-area electronic devices for organic photovoltaics, organic light-emitting diodes, and organic field-effect transistors (OFETs).[1−3] For high-performance organic electronics, new π-conjugated platforms should be developed.[4−6] Among them, quinoid molecules have been extensively studied due to their interesting electronic states, superior electrical performance, and unique spin characteristics.[7−10] They possess planar and rigid structures with negligible torsional angles due to the double bond linkages between each ring, showing reduced bond length alternation (BLA) and well-delocalized π-electron pathway, as compared to aromatic analogues. These features are favorable for $\pi-\pi$ stacking in the solid state, leading to efficient charge-transport properties.[11]

To establish a quinoidal structure, electron-withdrawing groups (EWGs) should be used at termini. A few EWGs are used for the terminal groups of quinoidal molecules such as dicyanomethylene (DCM), quinone, carbonyl, and *para*-quinodimethane, as shown in Figure 1.[12−14] The DCM group is generally used for quinoidal oligothiophenes with high performance in OFET devices.[15−17] However, the DCM-terminated quinoidal molecules require rather complex procedures, including the preparation of dibrominated aromatic compounds, Pd-catalyzed Takahashi coupling reaction, and oxidation of bis(dicyanomethyl)-precursors by 2,3-dichloro-5,6-dicyano-1,4-benzoquinone.[18,19]

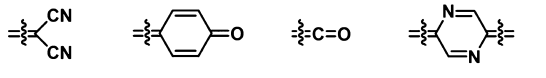

Figure 1. Specific terminal groups for the quinoid structure.

Received: August 2, 2021
Accepted: September 23, 2021
Published: October 7, 2021

Scheme 1. Synthesis of BzTQuT and QuT

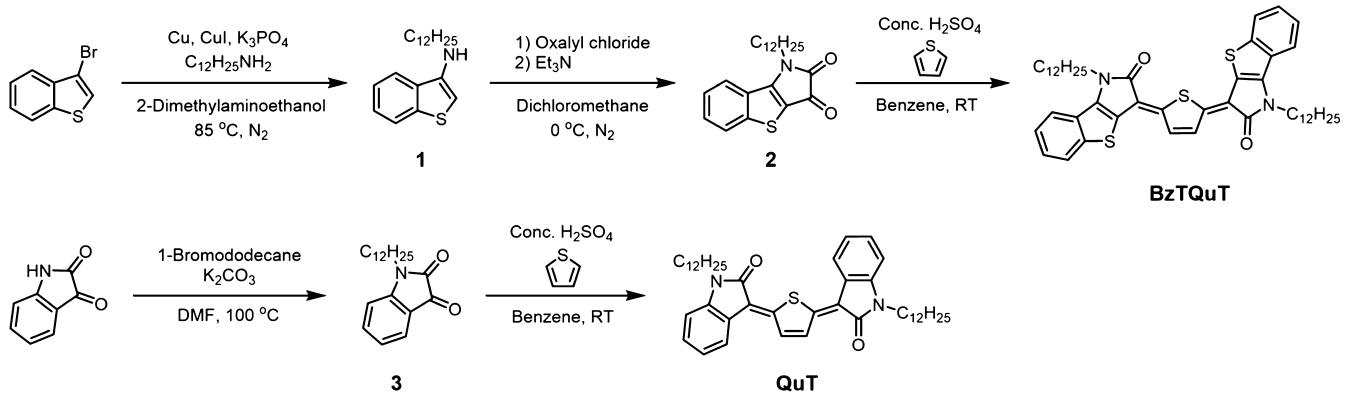

Isatin contains electron-withdrawing γ-lactam groups, which is also used as terminal groups for the formation of a quinoidal platform. Isatin-terminated quinoids have recently been reported owing to their advantages of good solubility in organic solvents via *N*-alkylation and the possibility of diverse modification of both quinoidal cores and termini.[20] Moreover, they could be synthesized by facile short steps under ambient conditions without any metal catalyst via the indophenine reaction between thiophene and isatin derivatives.[21−23] Most reports have focused on tailoring quinoidal cores from a common thiophene to benzene-annelated, fused and/or thiophene-*S*,*S*-dioxide derivatives.[24−28] However, there has been little research on the property changes of quinoidal molecules depending on the structural refinement of terminal isatin units so far.

In this study, we designed and synthesized benzothiophene-ended quinoidal thiophene (BzTQuT) and quinoidal thiophene (QuT) using modified and original isatin units to verify the effect of introducing a fused ring into the termini of quinoidal molecules. The electronic states of the two quinoidal molecules were characterized by Raman spectroscopy and density functional theory (DFT) calculations. Their optical and electrochemical properties were measured by UV−vis−NIR absorption and cyclic voltammetry (CV). BzTQuT showed reduced BLA and lowered band gap compared to QuT. When BzTQuT was applied to OFET devices as an active layer, they exhibited p-type charge transport with a relatively low hole mobility due to film morphology. A small-molecule/polymer blend system was used to improve the morphology, which is beneficial for charge transport. The OFET devices based on a BzTQuT/poly(2-vinylnaphtalene) (PVN) blend film showed a hole mobility of up to 0.09 $cm^2 V^{-1} s^{-1}$.

2. RESULTS AND DISCUSSION

2.1. Synthesis. The synthesis procedures of quinoidal small molecules are shown in Scheme 1. BzTQuT was successfully synthesized in only three steps. A linear dodecyl alkyl chain was introduced to 3-bromobenzo[*b*]thiophene through the Ullmann reaction to achieve good solubility and induce effective packing in the solid state. Next, *N*-dodecylbenzo[*b*]thiophen-3-amine (**1**) was converted into *N*-dodecylbenzo[4,5]thieno[3,2-*b*]pyrrole-2,3-dione (**2**) via cyclization using oxalyl chloride. Finally, BzTQuT was produced by the nucleophilic addition of thiophene to the ketone moiety of 2 using concentrated sulfuric acid, yielding in 13%. QuT was synthesized using pristine isatin. First, dodecyl alkyl side chains were incorporated at the *N*-position of isatin under basic conditions. Subsequently, QuT was prepared by *N*-dodecylisatin (**3**) according to the procedure for the synthesis of BzTQuT, yielding in 12%. The synthesized quinoidal molecules were confirmed by ^{1}H NMR, elemental analysis (EA), and matrix-assisted laser desorption/ionization time-of-flight mass spectrometry (MALDI-TOF-MS) (Figure S1). Both BzTQuT and QuT have three geometrical isomers, owing to the two double bonds in the quinoidal core. As shown in nuclear magnetic resonance (NMR) spectra, both quinoidal molecules remain as the mixture of geometrical isomers. As confirmed in our previous research, QuT with an asymmetric structure is known as a major isomer because it has the smallest diploe moment.[11] BzTQuT exhibited a doublet proton peak at 8.62 ppm in the NMR spectrum, caused by a proton close to an oxygen atom of the γ-lactam group into the quinoidal thiophene core in case of an asymmetric (*E*, *Z*) form. An integral ratio of this peak was 0.34, when the peak of two protons positioned at the carbon adjacent nitrogen atom into the isatin derivatives was selected as a reference. Therefore, BzTQuT with the (*E*, *Z*) form is also considered a major isomer with 68% in chloroform at room temperature. Unfortunately, a single isomer was difficult to be isolated because the isomerization of BzTQuT and QuT seems to take place at room temperature under visible light.[11,20] We speculated that an open-shell diradical state contributed to isomerization under ambient conditions. Because of the interconversion between the closed-shell quinoid and open-shell diradical structures, the double bond linkages in the quinoidal core can be switched into single bonds, resulting in the rotation of bonds and isomerization.[29]

2.2. DFT Calculation. DFT calculations were initially conducted to estimate the optimized geometries and Frontier molecular orbital energy levels of the two quinoidal molecules (Figure 2). Dodecyl alkyl side chains were replaced with methyl groups for computational simplicity. All BzTQuT and QuT exhibited highly planar structures with negligible torsional angles, which might be beneficial for π−π stacking. The calculated highest occupied molecular orbital (HOMO) and lowest unoccupied molecular orbital (LUMO) energy levels of BzTQuT and QuT were −5.01, −3.23 and −5.52, −3.15 eV, respectively. The calculated band gap of BzTQuT was much smaller than that of QuT due to reduced BLA, which is consistent with the results of Raman analysis, as will be described below. BzTQuT showed an increased HOMO level, which was ascribed to additional donating thiophene units in terminal benzothiophenes.[30] The HOMO levels of the

https://doi.org/10.1021/acsomega.1c04120
ACS Omega 2021, 6, 27305−27314

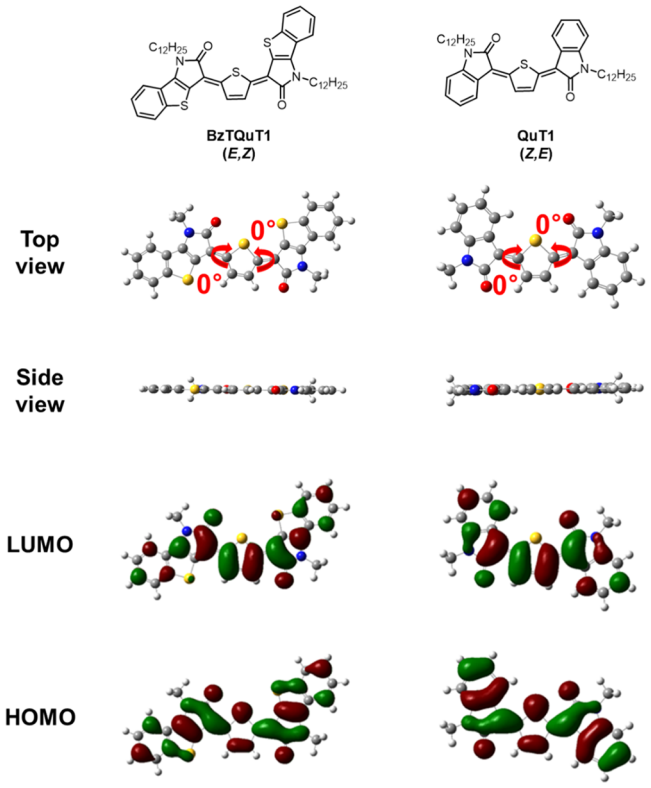

Figure 2. Optimized geometries and Frontier molecular orbitals of (a) BzTQuT and (b) QuT.

two quinoidal molecules showed well-delocalized orbitals, which could be beneficial for hole transport.

2.3. Raman Analysis and Bond Length Calculation. Raman spectroscopy was conducted with a 532 nm laser to understand the electronic structure of each molecule. According to the effective conjugation coordinate theory, conjugated molecules tend to show an intense collective vibration Raman band as the main peak due to the intrinsic polarizability of π-electrons. When the backbone of conjugated molecules is extended, extended effective π-conjugation length and reduced BLA provoke redistribution of C=C/C−C bonds with a frequency downshift of the ν(C=C/C−C) vibration peaks.[31] In general, collective ν(C=C/C−C) vibration peaks are displayed in the 1300−1700 cm^{-1} region.[32] The Raman spectra of both quinoidal molecules were theoretically calculated by DFT, which was used to assist in understanding the experimental Raman analysis (Figure S2). As shown in Figure 3a, QuT exhibited two main Raman bands at 1542 and 1511 cm^{-1} in accordance with the simulated Raman spectra of QuT. The former corresponds to the C=C stretching vibration within the thiophene core, and the latter represents the collective ν(C=C/C−C) vibration in the quinoid structure (Figure S2b). On the other hand, BzTQuT showed an intense Raman peak at 1451 cm^{-1}. The intense Raman band of BzTQuT corresponds to the collective ν(C=C/C−C) vibration of the entire conjugated skeleton, as shown in the theoretical eigenvector in Figure S2c. The effective π-conjugation length was extended by the introduction of benzothiophene into the quinoidal molecule, leading to a drastically downshifted Raman peak of BzTQuT.[33] For BzTQuT, the Raman bands at 1523 and 1406 cm^{-1} were attributed to the vibration of the double bonds in the quinoidal core and the vibration of the double bond at the termini, respectively.

To further understand the dramatic shift of the collective Raman band of the two quinoidal molecules, the lengths of the carbon−carbon bonds in the quinoidal core were calculated at the B3LYP/6-311G(d,p) level using Gaussian 09. As shown in Figure 3b, BzTQuT showed shorter single bonds and longer double bonds compared to QuT, leading to reduced BLA, as compared to QuT. This suggested that the effective π-conjugation length was extended for BzTQuT, in agreement with the results of Raman analysis in which the collective Raman band for BzTQuT was downshifted.

2.4. Thermal Properties. Thermal properties were evaluated by thermogravimetric analysis (TGA) and differential scanning calorimetry (DSC). The thermal properties of BzTQuT and QuT are summarized in Table S1. Both quinoidal small molecules exhibited sufficient thermal stability for device fabrication. BzTQuT and QuT displayed T_d values of 327 and 265 °C, respectively (Figure S3). The higher T_d of BzTQuT indicates better thermal stability than that of QuT. DSC analysis was performed to investigate the thermal behavior of the quinoidal small molecules (Figure 4). BzTQuT exhibited two reversible endothermic and exothermic transition peaks in the 30−120 °C range, which is indicative of liquid-crystalline-like behavior arising from the rigid rod structure.[34,35] On the first heating and cooling process, the melting temperature (T_m) and the crystalline temperature (T_c) were observed at 160 and 115 °C, respectively. On the second heating process, T_m was slightly changed and split to 144 and 157 °C, which might have originated from the formation of a crystalline polymorph during first cooling. QuT showed T_m at 114 °C and T_c at 56 °C on the first heating and cooling

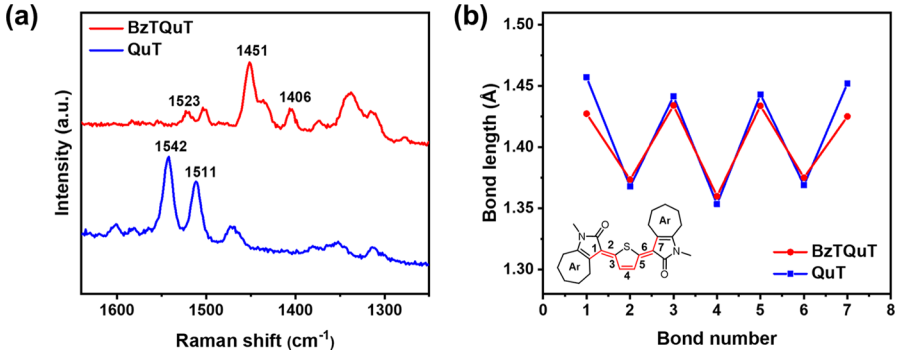

Figure 3. (a) Resonant Raman spectra at 532 nm of BzTQuT and QuT. (b) Calculated length of carbon−carbon bonds in BzTQuT and QuT.

https://doi.org/10.1021/acsomega.1c04120
ACS Omega 2021, 6, 27305−27314

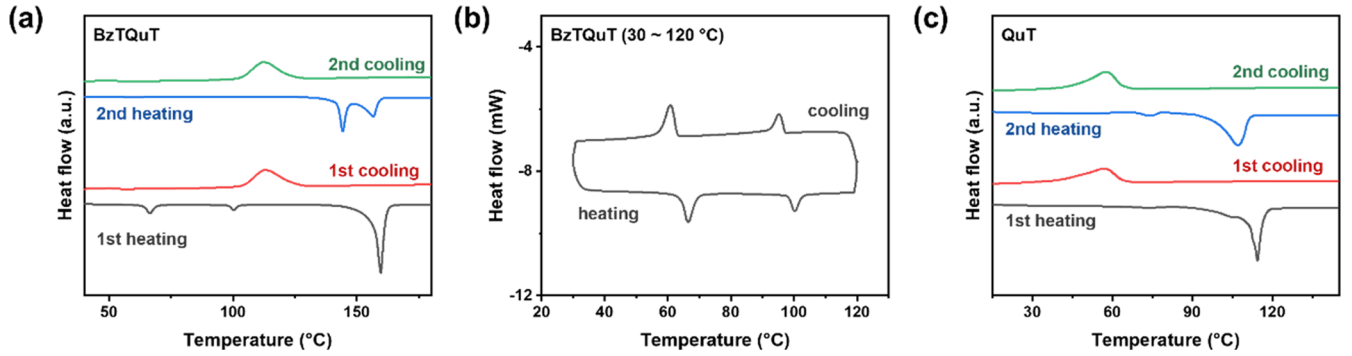

Figure 4. DSC curves of (a) BzTQuT, (b) BzTQuT in the 30−120 °C range, and (c) QuT.

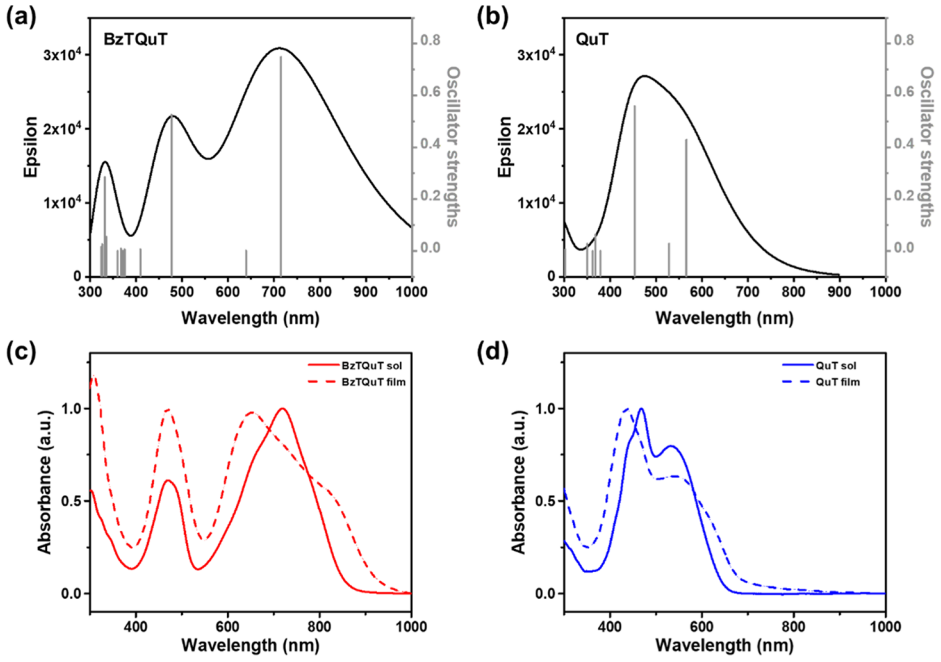

Figure 5. Simulated absorption spectra of (a) BzTQuT and (b) QuT as a single molecule using B3LYP TD-DFT/6-311^{++}G(d,p) with Gaussian 09. UV−Vis−NIR absorption spectra of (c) BzTQuT and (d) QuT in a dilute solution and as thin films.

Table 1. Summary of Optical and Electrochemical Properties of BzTQuT and QuT

	λ_{max} (sol.) [nm]	λ_{max} (film) [nm]	λ_{onset} (film) [nm]	E_g^{opt} [eV]	HOMO [eV]	LUMO [eV]	E_g^{cv}[a] [eV]
BzTQuT	470, 719	469, 653	928	1.34	−5.19	−3.70	1.49
QuT	468, 533	436, 540	681	1.82	−5.65	−3.65	2.00

[a] $E_g^{CV} = E_{LUMO} - E_{HOMO}$.

process. BzTQuT showed a higher thermal transition temperature than QuT, which was attributed to its extended backbone.[36,37]

2.5. Optical and Electrochemical Properties. We first conducted time-dependent DFT (TD-DFT) calculations to predict the absorption spectra of BzTQuT and QuT in the gas phase (Figure 5a,b). For BzTQuT, the absorption band at approximately 470 nm was assigned to HOMO − 2 → LUMO, and HOMO → LUMO was attributed to the band at approximately 715 nm. QuT showed a similar feature; the first band around 453 nm was associated with HOMO − 2 → LUMO, and the second band around 566 nm was related to HOMO → LUMO (Table S2). The simulated absorption spectra well correlated with the experimental UV−vis−NIR absorption spectra in the solution.

UV−vis−NIR absorption spectra were measured to explore the optical properties of BzTQuT and QuT, as shown in Figure 5c,d. A summary of the material properties is presented in Table 1. The absorption spectra of BzTQuT were dramatically red-shifted compared to those of QuT. In addition, BzTQuT showed a small band gap of 1.34 eV despite the short quinoidal core length, representing a substantial increase in the effective conjugation length by the incorporation of extended fused rings. Interestingly, λ_{max} in the film of both quinoidal small molecules was blue-shifted compared to that in the solution. These optical properties could be considered as the result of H-aggregation, which is formed when the dimer is aligned side-by-side in parallel.[38] In H-aggregation, the excited energy level is split into two transition states induced by dipole coupling. Excitation from

https://doi.org/10.1021/acsomega.1c04120
ACS Omega 2021, 6, 27305−27314

the ground state to the lower level is forbidden, but transition to a higher energy level is allowed, resulting in blue-shifted absorption. Similar H-aggregation tendency has been reported for isatin-terminated and other quinoidal molecules, which could be attributed to high planarity and rigidity of the molecular structure.[22,39]

CV measurements were carried out using a degassed CH_3CN solution containing 0.1 M Bu_4NPF_6 as a support electrolyte. BzTQuT showed a quasi-reversible reduction and two quasi-reversible oxidation waves, and QuT showed a quasi-reversible reduction and a quasi-reversible oxidation waves (Figure S4). The HOMO and LUMO energy levels were calculated from the onset point of the first oxidation and reduction and calibrated against the ferrocene/ferrocenium couple. The HOMO/LUMO energy levels were found to be −5.19/−3.70 eV for BzTQuT and −5.65/−3.65 eV for QuT. This indicated that BzTQuT is easier to be oxidized than QuT, which is ascribed to electron-donating properties of additional thiophene units in BzTQuT. The electrochemical band gaps of BzTQuT and QuT are 1.49 and 2.00 eV, respectively. These results were consistent with the optical band gap and DFT calculations. The smaller band gap of BzTQuT was associated with reduced BLA by the longer π-conjugation length and the higher HOMO energy level originating from the electron-rich nature of additional thiophene units.

2.6. Charge Transporting Properties. The electrical characteristics were confirmed by the fabrication of OFETs. OFET devices were fabricated on a glass substrate in the configuration of top-gate/bottom-contact (TG/BC). BzTQuT and QuT were deposited by spin-coating with chlorobenzene and trichloroethylene solutions (15 mg mL^{-1}), respectively, and more experimental details are described in the experimental section. The device performance parameters are summarized in Table 2, and their representative output and transfer curves are shown in Figure S5. Unfortunately, OFETs based on QuT did not operate. This could be ascribed to the poor film-forming properties of the particularly small QuT molecule. The OFET devices based on BzTQuT showed only p-channel charge transport, arising from the electron-donating property of additional thiophenes at the termini. Unfortunately, the OFET devices based on films, both films in pristine and annealed at 150 °C, exhibited low hole mobilities below 10^{-3} cm^2 V^{-1} s^{-1}. In particular, an OFET device with a film annealed at 150 °C showed reduced mobility compared to that of the pristine film.

Table 2. Device Characteristics of OFETs Based on BzTQuT

	ann. temp. [°C]	mobility [cm^2 V^{-1} s^{-1}]	V_{th} [V]	I_{on}/I_{off}
BzTQuT	pristine	8.4×10^{-4} (1.1×10^{-3})[a]	9.5	10^2
	150	1.4×10^{-5} (6.9×10^{-4})[a]	−21.7	10^1

[a]Maximum mobility.

2.7. Film Morphology. To understand the device characteristics, the molecular orientation and crystallinity of the BzTQuT films were investigated by two-dimensional grazing-incidence wide-angle X-ray scattering (2D-GIWAXS). Images of 2D-GIWAXS are shown in Figure 6a,b, and the corresponding GIWAXS profiles are shown in Figure S6. The pristine film displayed highly ordered alkyl stacking diffraction peaks corresponding to lamellar stacking in both in-plane and out-of-plane directions, indicating a bimodal orientation. The first diffraction peaks were observed in both in-plane direction at q_{xy} = 0.25 $Å^{-1}$ with a distance of 25.2 Å and out-of-plane at q_z = 0.24 $Å^{-1}$ with an interlayer distance of 26.3 Å. The film annealed at 150 °C still showed strong alkyl stacking diffraction peaks in out-of-plane direction and revealed a clear dot pattern, indicating the presence of a highly crystalline phase. Moreover, intense diffraction peaks were revealed in in-plane direction in the annealed film (Figure S6a). The *d*-spacing extracted from the first diffraction peak is 16.9 Å, which is close to the calculated length of BzTQuT in the long axis direction (18.8 Å). BzTQuT has a highly planar structure and possesses an extended backbone by benzothiophene termini, leading to the formation of a highly crystalline phase by post-thermal treatment.

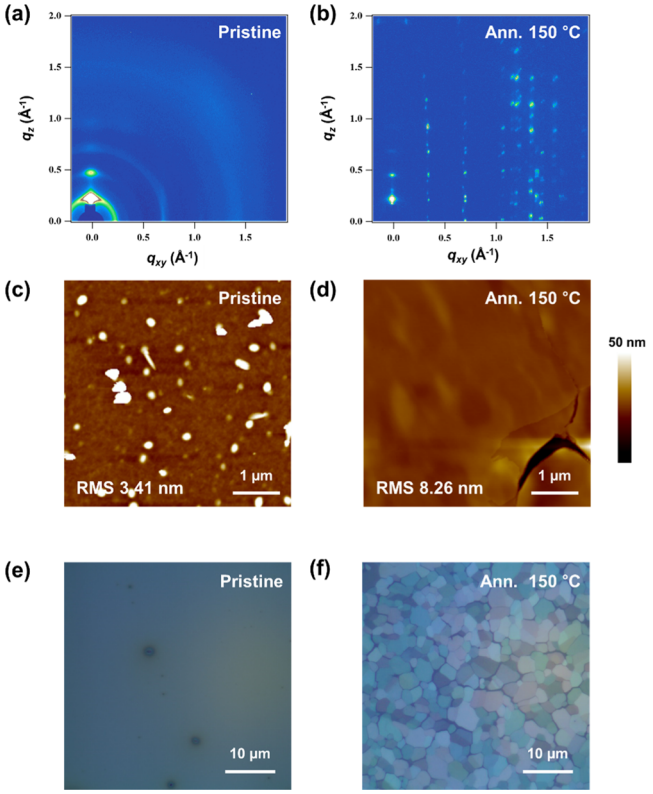

Figure 6. (a,b) 2D-GIWAXS images; (c,d) AFM images; and (e,f) POM images of pristine BzTQuT films (a,c,e) and those annealed at 150 °C (b,d,f).

The surface morphology was investigated by atomic force microscopy (AFM) and polarized optical microscopy (POM). The pristine BzTQuT film showed obtrusive particles and a rather large root-mean-square (rms) roughness of 3.41 nm in the AFM image, and its POM image was featureless (Figure 6c,e). In the AFM image of the film annealed at 150 °C, large crystalline domains and deep grain boundaries were observed, and rms roughness increased up to 8.26 nm (Figure 6d). In addition, the POM image of this film also featured well-developed microscale polycrystalline domains (Figure 6f), which is well consistent with the 2D-GIWAXS analysis. However, large grain boundaries were also observed. This discontinuous morphology could adversely affect the charge transport, leading to diminished mobility in the OFET devices.[40−42]

https://doi.org/10.1021/acsomega.1c04120
ACS Omega 2021, 6, 27305−27314

2.8. Blend with Amorphous Insulating Polymers. To improve the device performance, OFET devices based on small-molecule/polymer blend films were fabricated. When small molecules are blended with an amorphous insulating polymer as a binder, a morphology with high uniformity can be obtained by controlling the dewetting nature of small molecules and increasing the interconnectivity of grains, leading to an enhancement of the device performance and uniformity.[43−45] The quinoidal small molecule, BzTQuT, was blended with amorphous insulating polymers: polystyrene (PS) and PVN. OFETs with the TG/BC configuration were fabricated using a blend solution, which was prepared using 1,2-dichlorobenzene (*o*-DCB) with 10 mg mL^{-1} in a 1:1 ratio by weight. The device performance of all OFETs based on the blend films was improved when compared to that of the BzTQuT neat films (Figure 7 and Table 3). The best mobility

Table 3. Device Characteristics of OFETs Based on BzTQuT/PVN and BzTQuT/PS Blend Films

	ann. temp. [°C]	mobility [cm^2 V^{-1} s^{-1}]	V_{th} [V]	I_{on}/I_{off}
BzTQuT/PVN = 1:1	pristine	0.013 (0.022)[a]	−18.4	10^4
	150	0.088 (0.090)[a]	−15.0	10^2
BzTQuT/PS = 1:1	pristine	5.7×10^{-3} (0.018)[a]	−21.0	10^2
	150	0.022 (0.043)[a]	−15.9	10^2

[a]Maximum mobility.

of 0.09 cm^2 V^{-1} s^{-1} was achieved for the BzTQuT/PVN blend film annealed at 150 °C. Interestingly, the OFET devices based on both blend films annealed at 150 °C showed improved mobility, which is 2 orders of magnitude higher than that of the OFETs based on the BzTQuT neat films.

AFM analysis was performed to investigate the surface morphology of blend films, and AFM images of the films blended with PVN and PS are shown in Figure 8. Pristine films blended with both PVN and PS exhibited smoother surface morphology without any particles and lower rms roughness values than a neat BzTQuT film (3.41 nm). Two PVN- and PS-based blend films annealed at 150 °C showed lower rms roughness values of 0.841 and 0.147 nm, respectively, compared to each blend film in the pristine and neat annealed film (8.26 nm) particularly. For the BzTQuT/PVN blend film annealed at 150 °C, the microscale polycrystalline domain was still observed; however, the grain boundaries between the crystalline domains remarkably diminished. This indicate that a decrease of structural defects such as grain boundaries leads to enhanced charge transport properties, which is consistent with the result of the device performance.[46,47] These results demonstrate that the small-molecule/polymer blend is an effective strategy for improving the device performance.

3. CONCLUSIONS

In this study, BzTQuT was successfully synthesized by introducing benzothiophene into the isatin termini via only three steps and characterized in comparison with QuT. BzTQuT with fused rings showed a downshifted collective Raman band and smaller band gap, indicating that the effective conjugation length was well extended. The additional thiophene unit in BzTQuT led to a higher HOMO energy level owing to the electron-donating properties of thiophene, as compared to QuT. OFET devices based on BzTQuT exhibited p-type charge transport with low hole mobility in both pristine and annealed films. In particular, an OFET based on an annealed film showed reduced mobility, as compared to the pristine film, which was attributed to the deep grain boundary between large crystalline domains. Improvements in the device performance were achieved by BzTQuT blended with an insulating polymer binder. In a device based on a BzTQuT/PVN blend film, the hole mobility was increased up to 0.09 cm^2 V^{-1} s^{-1} under the same annealing condition. The incorporation of extended fused rings as termini could be an effective strategy to lower the band gap and to improve the charge transport properties.

4. EXPERIMENTAL SECTION

4.1. Materials and Methods. All chemical reagents were purchased from Sigma-Aldrich, Alfa Aesar, and TCI and used without purification. Gas chromatography−mass spectrometry measurements were performed on a Clarus 690/Clarus SQ 8 T instrument from PerkinElmer. MALDI-TOF-MS was carried out by Bruker Autoflex speed using α-cyano-4-hydroxycinnamic acid as the matrix. EA was performed on UNICUBE (Elementar). ^{1}H NMR spectra were recorded on a 400 MHz JEOL JNM ECX400 spectrometer. TGA was conducted on a TGA 4000 (PerkinElmer) instrument at a heating rate of 10 °C min^{-1} under nitrogen. DSC was performed using a Q20 instrument (TA instrument) at a heating rate of 10 °C min^{-1} under nitrogen. UV−vis−NIR absorption spectra were obtained using a PerkinElmer LAMBDA 750 UV−vis−NIR spectrophotometer. The solution was prepared using chlorobenzene and trichloroethylene at a concentration of ∼10^{-5} M for BzTQuT and QuT, respectively. The films were spin-coated onto a glass substrate using a small-molecule solution of 15 mg mL^{-1}, and thermal annealing was performed for 20 min. A small-molecule/polymer blend solution was prepared at 10 mg mL^{-1} in *o*-DCB. The solution was deposited onto a glass substrate and thermally annealed for 30 min. CV was performed using an Eco Chemie Autolab PGSTAT30 instrument at a scan rate of 50 mV s^{-1}. BzTQuT and QuT films were tested in a degassed 0.1 M Bu_4NPF_6/acetonitrile solution. An indium tin oxide electrode coated with the quinoidal molecule film was used as the working electrode, an Ag/AgCl electrode was used as the reference electrode, and platinum was used as the counter electrode. Raman spectra were obtained using an Andor Shamrock SR-500i-A spectrometer (Andor Tech) equipped with a charge-coupled device camera (DV420A-OE, Andor Tech) and a 532 nm laser (SDL-532 = 200T, Shanghai Dream Lasers Technology Co., Ltd.). AFM measurements were performed using a Nanoscope III (Veeco Instrument, Inc.) instrument in tapping mode. 2D-GIWAXS was performed using the synchrotron radiation source 9A beamline at the Pohang Accelerator Laboratory (PAL). POM images were obtained by Axio Scope A1 (Carl Zeiss, Germany).

4.2. Material Synthesis. *4.2.1. Synthesis of N-Dodecylbenzo[b]thiophen-3-amine (1).* 3-Bromobenzo[*b*]-thiophene (5.0 g, 23.46 mmol), dodecylamine (5.22 g, 28.15 mmol), copper (74.0 mg, 1.17 mmol), copper iodide (0.22 g, 1.17 mmol), and tripotassium phosphate (9.96 g, 46.92 mmol) were dissolved in 2-dimethylaminoethanol (45 mL) under a nitrogen atmosphere and heated with stirring at 85 °C for 48 h. After cooling to room temperature, the mixture was filtered and evaporated under reduced pressure. The residue was purified using column chromatography with hexane/methylene

https://doi.org/10.1021/acsomega.1c04120
ACS Omega 2021, 6, 27305−27314

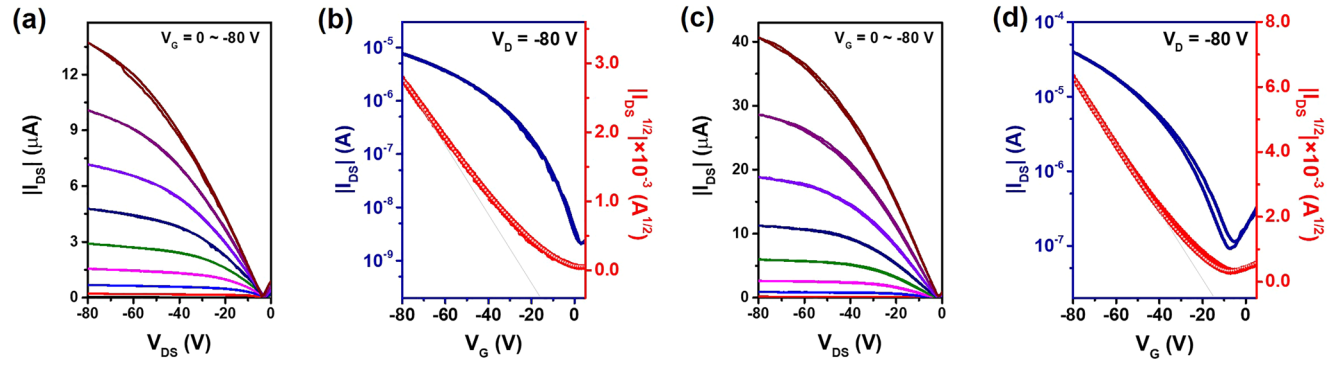

Figure 7. (a,c) Representative output curves and (b,d) transfer curves of OFET devices based on pristine BzTQuT/PVN films (a,b) and those annealed at 150 °C (c,d).

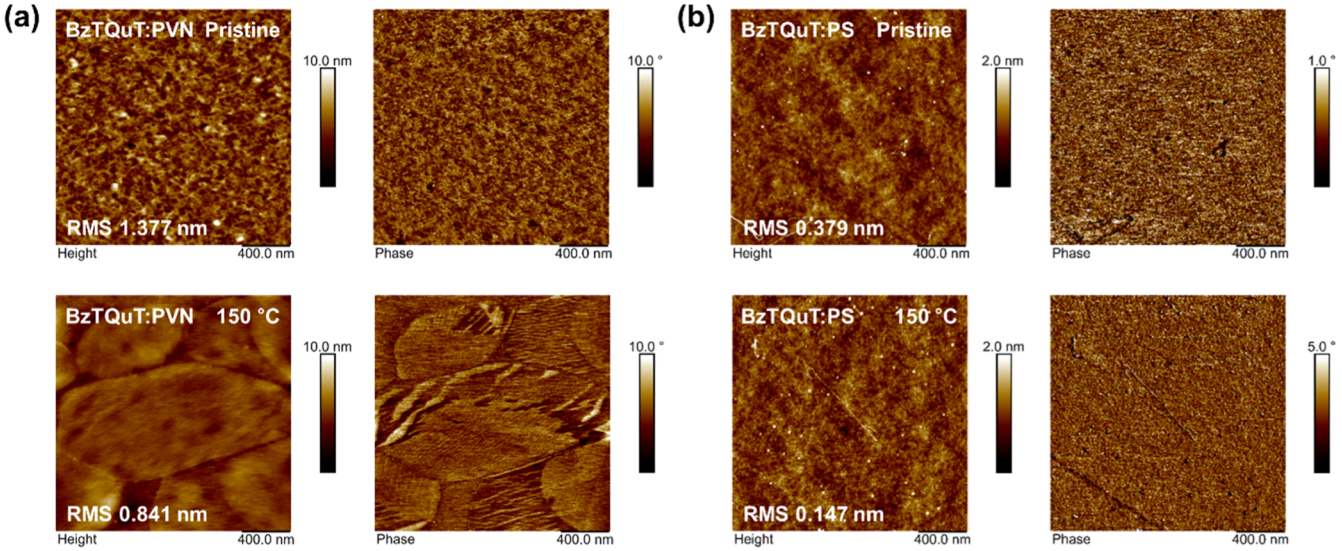

Figure 8. AFM images of (a) BzTQuT/PVN and (b) BzTQuT/PS blend films (upper: in pristine; bottom: annealed at 150 °C).

chloride (3:1, v/v) as the eluent to obtain compound **1** (2.50 g, yield: 33%) of a white solid. MS (EI, *m*/*z*): $[M]^+$ calcd for $C_{20}H_{31}NS$, 317.22; found, 317; ^1H NMR (400 MHz, $CDCl_3$): δ (ppm) 7.80−7.73 (m, 1H), 7.59−7.51 (m, 1H), 7.37−7.30 (m, 2H), 6.03 (s, 1H), 3.80 (s, 1H), 3.22 (t, J = 7.1 Hz, 2H), 1.80−1.66 (m, 2H), 1.50−1.20 (m, 18H), 0.88 (t, J = 6.8 Hz, 3H).

*4.2.2. Synthesis of N-Dodecyl-1H-benzo[4,5]thieno[3,2-b]pyrrole-2,3-dione (**2**).* Oxalyl chloride (0.23 mL, 2.70 mmol) was added to methylene chloride (10 mL) and stirred at 0 °C for 30 min under nitrogen. *N*-dodecylbenzo[*b*]thiophen-3-amine (1) (661 mg, 2.08 mmol) was dissolved in methylene chloride (4 mL) dropwise. After stirring for 30 min, triethylamine (1.3 mL, 9.7 mmol) was diluted in methylene chloride (4 mL) and added dropwise to the mixture. The ice bath was removed after 10 min, and the mixture was stirred at room temperature overnight. The reaction mixture was evaporated under reduced pressure to remove the solvent and residual triethylamine. The residue was filtered and purified using flash column chromatography with hexane/ethyl acetate (8:1, v/v) to obtain red solid compound **2** (0.19 g, yield: 25%). MS (EI, *m*/*z*): $[M]^+$ calcd for $C_{22}H_{29}NO_2S$, 371.19; found, 371; ^1H NMR (400 MHz, $CDCl_3$): δ (ppm) 7.92−7.85 (m, 2H), 7.57 (m, 1H), 7.49 (m, 1H), 3.99 (t, J = 7.2 Hz, 2H), 1.84−1.74 (m, 2H), 1.48−1.20 (m, 18H), 0.88 (t, J = 6.9 Hz, 3H).

4.2.3. Synthesis of Benzothiophene-Ended Quinoidal Thiophene (BzTQuT). *N*-Dodecylbenzo[4,5]thieno[3,2-*b*]-pyrrole-2,3-dione (192.8 mg, 0.52 mmol) and thiophene (87.3 mg, 1.04 mmol) were dissolved in benzene. Subsequently, concentrated sulfuric acid (0.03 mL, 0.52 mmol) was added dropwise. The reaction mixture was stirred for 3 h, and water was poured. The mixture was extracted with chloroform and dried over $MgSO_4$. After removing the solvent under reduced pressure, the product was purified using column chromatography with hexane/chloroform (5:1, v/v) as the eluent, yielding 52.7 mg (13%) of a green solid. MS (MALDI-TOF, *m*/*z*): $[M + H]^+$ calcd for $C_{48}H_{60}N_2O_2S_3$, 793.39; found, 793.40; EA: Anal. Calcd for $C_{48}H_{60}N_2O_2S_3$: C, 72.68; H, 7.62; N, 3.53; O, 4.03; S, 12.13%. Found: C, 72.68; H, 8.11; N, 3.24; O, 4.54; S, 11.48%.

*4.2.4. Synthesis of 1-Dodecylindoline-2,3-dione (**3**).* Isatin (5.0 g, 33.98 mmol) and K_2CO_3 (9.4 g, 67.96 mmol) were dissolved in anhydrous *N*,*N*-dimethylformamide (150 mL) and stirred at 100 °C under a nitrogen atmosphere. 1-Boromododecane (12.7 g, 50.97 mmol) was diluted with anhydrous *N*,*N*-dimethylformamide (50 mL) and poured into the mixture. The solution was then stirred overnight. After cooling to room temperature, the reaction mixture was extracted with methylene chloride and water, and the combined organic layer was dried over $MgSO_4$. The mixture was filtered and purified using column chromatography with

https://doi.org/10.1021/acsomega.1c04120
ACS Omega 2021, 6, 27305−27314

hexane/methylene chloride (2:1, v/v) as the eluent to yield compound **3** (8.06 g, yield: 75%) of an orange solid. MS (EI, m/z): $[M]^+$ calcd for $C_{20}H_{29}NO_2$, 315.22; found, 315.0; ^1H NMR (400 MHz, $CDCl_3$): δ (ppm) 7.63−7.54 (m, 2H), 7.15−7.06 (m, 1H), 6.89 (m, 1H), 3.75−3.68 (t, J = 7.2 Hz, 2H), 1.76−1.63 (m, 2H), 1.43−1.19 (m, 18H), 0.88 (t, J = 6.8 Hz, 3H).

4.2.5. Synthesis of Quinoidal Thiophene (QuT). QuT was prepared according to the procedure for the synthesis of BzTQuT, yielding a 12% red solid. MS (MALDI-TOF, m/z): $[M + H]^+$ calcd $C_{44}H_{60}N_2O_2S$, 681.44; found, 681.43. EA: Anal. Calcd for $C_{44}H_{60}N_2O_2S$: C, 77.60; H, 8.88; N, 4.11; O, 4.70; S, 4.71%. Found: C, 78.00; H, 9.30; N, 3.74; O, 4.95; S, 4.71%.

4.3. DFT Calculation. DFT calculations for the geometry optimization and prediction of the Raman spectra of the molecules were performed at the B3LYP/6-311^{++}G(d,p) level of theory using Gaussian 09 software. For computational simplicity, this simulation was carried out with methyl groups instead of dodecyl alkyl chains. TD-DFT was carried out at the same level of theory to evaluate the transition energy and the oscillator strength, and simulated UV−vis absorption spectra were obtained.

4.4. Device Fabrication. TG/BC OFETs were fabricated to investigate the charge transport properties of the molecules. Au and Ni (15 and 3 nm-thick, respectively) were patterned onto Corning Eagle 2000 glass substrates using photolithography to fabricate source and drain electrodes, respectively, with a channel length (L) of 20 μm and a channel width (W) of 1.0 mm. The patterned substrates were cleaned in an ultrasonication bath with deionized water, acetone, and isopropyl alcohol for 10 min. Next, the substrates were dried in an oven to remove the residual solvent. The prepared substrates were then exposed to UV/ozone for 30 min. The fabrication of OFET devices was carried out in a N_2-filled glovebox. BzTQuT was dissolved in chlorobenzene (15 mg mL^{-1}). The active layer was deposited onto the substrate by spin-coating at 1500 rpm (3 s acceleration) followed by thermal annealing at 150 °C for 20 min. A small-molecule/polymer blend solution was prepared using *o*-DCB at 10 mg mL^{-1} in a 1:1 ratio by weight. PVN and PS were used as binding polymers, and the weight-average molecular weights (M_w) were 175 kDa for PVN and 280 kDa for PS. The blend solution was stirred overnight at 100 °C in a hot plate for complete mixing. The blend solution was deposited onto the substrate at 500 rpm for 40 s, with 3 acceleration followed by 2000 rpm for 20 s, and then thermally treated at 150 for 30 min. Subsequently, CYTOP (Asahi Glass, capacitance: 4.8 nF cm^{-2}) was spin-coated as a dielectric layer and baked at 80 °C for 2 h 30 min. Al (50 nm-thick) was evaporated as a top gate by using a shadow mask. The OFET characterization was performed in a N_2-filled glovebox using a Keithley 4200-SCS instrument.

■ ASSOCIATED CONTENT

Supporting Information

The Supporting Information is available free of charge at https://pubs.acs.org/doi/10.1021/acsomega.1c04120.

NMR data, simulated Raman data, TD-DFT calculation for UV−vis absorption, TGA trace, CV graph, OFET characterization, and 2D-GIWAXS data (PDF)

■ AUTHOR INFORMATION

Corresponding Author

Dong-Yu Kim − *School of Materials Science and Engineering (SMSE), Research Institute for Solar and Sustainable Energies (RISE), Gwangju Institute of Science and Technology (GIST), Gwangju 61005, Republic of Korea;* orcid.org/0000-0003-2874-0329; Email: kimdy@gist.ac.kr

Authors

Yoonjung Mok − *School of Materials Science and Engineering (SMSE), Research Institute for Solar and Sustainable Energies (RISE), Gwangju Institute of Science and Technology (GIST), Gwangju 61005, Republic of Korea*

Yunseul Kim − *School of Materials Science and Engineering (SMSE), Research Institute for Solar and Sustainable Energies (RISE), Gwangju Institute of Science and Technology (GIST), Gwangju 61005, Republic of Korea*

Yina Moon − *School of Materials Science and Engineering (SMSE), Research Institute for Solar and Sustainable Energies (RISE), Gwangju Institute of Science and Technology (GIST), Gwangju 61005, Republic of Korea*

Jong-Jin Park − *School of Materials Science and Engineering (SMSE), Research Institute for Solar and Sustainable Energies (RISE), Gwangju Institute of Science and Technology (GIST), Gwangju 61005, Republic of Korea*

Yeonsu Choi − *School of Materials Science and Engineering (SMSE), Research Institute for Solar and Sustainable Energies (RISE), Gwangju Institute of Science and Technology (GIST), Gwangju 61005, Republic of Korea*

Complete contact information is available at: https://pubs.acs.org/10.1021/acsomega.1c04120

Author Contributions

†Y.M. and Y.K. contributed equally.

Notes

The authors declare no competing financial interest.

■ ACKNOWLEDGMENTS

This work was supported by Samsung Research Funding & Incubation Center of Samsung Electronics under Project number SRFC-MA1802-03 and the National Research Foundation of Korea (NRF) grant funded by Korea Government (NRF-2021R1A2B5B03086824). The authors acknowledge the Korea Basic Science Institute (KBSI) for providing the AFM measurement and the Pohang Accelerator Laboratory for providing a synchrotron radiation source at the 9A beamline to measure the 2D-GIWAXS used in this study.

■ ABBREVIATIONS

2D-GIWAXS, two-dimensional grazing-incidence wide-angle X-ray scattering; AFM, atomic force microscopy; BLA, bond-length-alternation; BzTQuT, benzothiophene quinoidal thiophene; CV, cyclic voltammetry; DSC, differential scanning calorimetry; DFT, density functional theory; EA, elemental analysis; HOMO, highest occupied molecular orbital; LUMO, lowest unoccupied molecular orbital; MALDI-TOF-MS, matrix-assisted laser desorption/ionization time-of-flight mass spectrometry; NMR, ^1H nuclear magnetic resonance; OFET, organic field-effect transistor; POM, polarized optical microscopy; PS, polystyrene; PVN, poly(2-vinylnaphtalene); TD-DFT, time-dependent density functional theory; TGA,

thermogravimetric analysis; TG/BC, top-gate/bottom-contact; QuT, quinoidal thiophene; *o*-DCB, 1,2-dichlorobenzene

REFERENCES

(1) Paterson, A. F.; Singh, S.; Fallon, K. J.; Hodsden, T.; Han, Y.; Schroeder, B. C.; Bronstein, H.; Heeney, M.; McCulloch, I.; Anthopoulos, T. D. Recent Progress in High-Mobility Organic Transistors: A Reality Check. *Adv. Mater.* **2018**, *30*, 1801079.

(2) Cheng, P.; Li, G.; Zhan, X.; Yang, Y. Next-generation organic photovoltaics based on non-fullerene acceptors. *Nat. Photonics* **2018**, *12*, 131−142.

(3) Bronstein, H.; Nielsen, C. B.; Schroeder, B. C.; McCulloch, I. The role of chemical design in the performance of organic semiconductors. *Nat. Rev. Chem.* **2020**, *4*, 66−77.

(4) Henson, Z. B.; Müllen, K.; Bazan, G. C. Design strategies for organic semiconductors beyond the molecular formula. *Nat. Chem.* **2012**, *4*, 699−704.

(5) Guo, X.; Baumgarten, M.; Müllen, K. Designing π-conjugated polymers for organic electronics. *Prog. Polym. Sci.* **2013**, *38*, 1832−1908.

(6) Gsänger, M.; Bialas, D.; Huang, L.; Stolte, M.; Würthner, F. Organic Semiconductors based on Dyes and Color Pigments. *Adv. Mater.* **2016**, *28*, 3615−3645.

(7) Casado, J.; Ponce Ortiz, R.; López Navarrete, J. T. Quinoidal oligothiophenes: new properties behind an unconventional electronic structure. *Chem. Soc. Rev.* **2012**, *41*, 5672−5686.

(8) Yuan, D.; Huang, D.; Rivero, S. M.; Carreras, A.; Zhang, C.; Zou, Y.; Jiao, X.; McNeill, C. R.; Zhu, X.; Di, C.-a.; Zhu, D.; Casanova, D.; Casado, J. Cholesteric Aggregation at the Quinoidal-to-Diradical Border Enabled Stable n-Doped Conductor. *Chem* **2019**, *5*, 964−976.

(9) Mikie, T.; Osaka, I. Small-bandgap quinoid-based π-conjugated polymers. *J. Mater. Chem. C* **2020**, *8*, 14262−14288.

(10) Zhang, C.; Zhu, X. n-Type Quinoidal Oligothiophene-Based Semiconductors for Thin-Film Transistors and Thermoelectrics. *Adv. Funct. Mater.* **2020**, *30*, 2000765.

(11) Kim, Y.; Hwang, H.; Kim, N.-K.; Hwang, K.; Park, J.-J.; Shin, G.-I.; Kim, D.-Y. π-Conjugated Polymers Incorporating a Novel Planar Quinoid Building Block with Extended Delocalization and High Charge Carrier Mobility. *Adv. Mater.* **2018**, *30*, 1706557.

(12) Asoh, T.; Kawabata, K.; Takimiya, K. Carbonyl-Terminated Quinoidal Oligothiophenes as p-Type Organic Semiconductors. *Materials* **2020**, *13*, 3020.

(13) Velusamy, A.; Yu, C. H.; Afraj, S. N.; Lin, C. C.; Lo, W. Y.; Yeh, C. J.; Wu, Y. W.; Hsieh, H. C.; Chen, J.; Lee, G. H.; Tung, S. H.; Liu, C. L.; Chen, M. C.; Facchetti, A. Thienoisoindigo (TII)-Based Quinoidal Small Molecules for High-Performance n-Type Organic Field Effect Transistors. *Adv. Sci.* **2021**, *8*, 2002930.

(14) Liu, X.; He, B.; Anderson, C. L.; Kang, J.; Chen, T.; Chen, J.; Feng, S.; Zhang, L.; Kolaczkowski, M. A.; Teat, S. J.; Brady, M. A.; Zhu, C.; Wang, L.-W.; Chen, J.; Liu, Y. para-Azaquinodimethane: A Compact Quinodimethane Variant as an Ambient Stable Building Block for High-Performance Low Band Gap Polymers. *J. Am. Chem. Soc.* **2017**, *139*, 8355−8363.

(15) Zhang, F.; Hu, Y.; Schuettfort, T.; Di, C.-a.; Gao, X.; McNeill, C. R.; Thomsen, L.; Mannsfeld, S. C. B.; Yuan, W.; Sirringhaus, H.; Zhu, D. Critical role of alkyl chain branching of organic semiconductors in enabling solution-processed N-channel organic thin-film transistors with mobility of up to 3.50 $cm^2 V^{-1} s^{-1}$. *J. Am. Chem. Soc.* **2013**, *135*, 2338−2349.

(16) Nakano, M.; Osaka, I.; Takimiya, K. Dibenzo[a,e]pentalene-embedded dicyanomethylene-substituted thienoquinoidals for n-channel organic semiconductors: synthesis, properties, and device characteristics. *J. Mater. Chem. C* **2015**, *3*, 283−290.

(17) Zhang, C.; Zang, Y.; Zhang, F.; Diao, Y.; McNeill, C. R.; Di, C.-a.; Zhu, X.; Zhu, D. Pursuing High-Mobility n-Type Organic Semiconductors by Combination of "Molecule-Framework" and "Side-Chain" Engineering. *Adv. Mater.* **2016**, *28*, 8456−8462.

(18) Xia, D.; Keerthi, A.; An, C.; Baumgarten, M. Synthesis of a quinoidal dithieno[2,3-d;2′,3′-d]benzo[2,1-b;3,4-b′]-dithiophene based open-shell singlet biradicaloid. *Org. Chem. Front.* **2017**, *4*, 18−21.

(19) Yamamoto, K.; Kato, S.-i.; Zajaczkowska, H.; Marszalek, T.; Blom, P. W. M.; Ie, Y. Effects of fluorine substitution in quinoidal oligothiophenes for use as organic semiconductors. *J. Mater. Chem. C* **2020**, *8*, 3580−3588.

(20) Kim, Y.; Kim, Y.-J.; Kim, Y.-A.; Jung, E.; Mok, Y.; Kim, K.; Hwang, H.; Park, J.-J.; Kim, M.-G.; Mathur, S.; Kim, D.-Y. Open-Shell and Closed-Shell Quinoid−Aromatic Conjugated Polymers: Unusual Spin Magnetic and High Charge Transport Properties. *ACS Appl. Mater. Interfaces* **2021**, *13*, 2887−2898.

(21) Tormos, G. V.; Belmore, K. A.; Cava, M. P. The indophenine reaction revisited. Properties of a soluble dialkyl derivative. *J. Am. Chem. Soc.* **1993**, *115*, 11512−11515.

(22) Hwang, H.; Khim, D.; Yun, J.-M.; Jung, E.; Jang, S.-Y.; Jang, Y. H.; Noh, Y.-Y.; Kim, D.-Y. Quinoidal Molecules as a New Class of Ambipolar Semiconductor Originating from Amphoteric Redox Behavior. *Adv. Funct. Mater.* **2015**, *25*, 1146−1156.

(23) Hu, Q.; Jiang, H.; Cui, Z.; Chen, W. An insight into the effect of S,S-dioxided thiophene on the opto-physical/electro-chemical properties and light stability for indophenine derivatives. *Dyes Pigm.* **2020**, *173*, 107891.

(24) Deng, Y.; Sun, B.; He, Y.; Quinn, J.; Guo, C.; Li, Y. Thiophene-S,S-dioxidized Indophenine: A Quinoid-Type Building Block with High Electron Affinity for Constructing n-Type Polymer Semiconductors with Narrow Band Gaps. *Angew. Chem., Int. Ed.* **2016**, *55*, 3459−3462.

(25) Yamamoto, K.; Ie, Y.; Nitani, M.; Tohnai, N.; Kakiuchi, F.; Zhang, K.; Pisula, W.; Asadi, K.; Blom, P. W. M.; Aso, Y. Oligothiophene quinoids containing a benzo[c]thiophene unit for the stabilization of the quinoidal electronic structure. *J. Mater. Chem. C* **2018**, *6*, 7493−7500.

(26) Huang, J.; Lu, S.; Chen, P.-A.; Wang, K.; Hu, Y.; Liang, Y.; Wang, M.; Reichmanis, E. Rational Design of a Narrow-Bandgap Conjugated Polymer Using the Quinoidal Thieno[3,2-b]thiophene-Based Building Block for Organic Field-Effect Transistor Applications. *Macromolecules* **2019**, *52*, 4749−4756.

(27) Hwang, K.; Lee, M.-H.; Kim, J.; Kim, Y.-J.; Kim, Y.; Hwang, H.; Kim, I.-B.; Kim, D.-Y. 3,4-Ethylenedioxythiophene-Based Isomer-Free Quinoidal Building Block and Conjugated Polymers for Organic Field-Effect Transistors. *Macromolecules* **2020**, *53*, 1977−1987.

(28) Yamamoto, K.; Jinnai, S.; Takehara, T.; Suzuki, T.; Ie, Y. Quinoidal Oligothiophenes Having Full Benzene Annelation: Synthesis, Properties, Structures, and Acceptor Application in Organic Photovoltaics. *Org. Lett.* **2020**, *22*, 547−551.

(29) Gopalakrishna, T. Y.; Zeng, W.; Lu, X.; Wu, J. From open-shell singlet diradicaloids to polyradicaloids. *Chem. Commun.* **2018**, *54*, 2186−2199.

(30) Chang, S.-L.; Hung, K.-E.; Cao, F.-Y.; Huang, K.-H.; Hsu, C.-S.; Liao, C.-Y.; Lee, C.-H.; Cheng, Y.-J. Isomerically Pure Benzothiophene-Incorporated Acceptor: Achieving Improved Voc and Jsc of Nonfullerene Organic Solar Cells via End Group Manipulation. *ACS Appl. Mater. Interfaces* **2019**, *11*, 33179−33187.

(31) Burrezo, P. M.; Zafra, J. L.; López Navarrete, J. T.; Casado, J. Quinoidal/Aromatic Transformations in π-Conjugated Oligomers: Vibrational Raman studies on the Limits of Rupture for π-Bonds. *Angew. Chem., Int. Ed.* **2017**, *56*, 2250−2259.

(32) Wood, S.; Hollis, J. R.; Kim, J.-S. Raman spectroscopy as an advanced structural nanoprobe for conjugated molecular semiconductors. *J. Phys. D: Appl. Phys.* **2017**, *50*, 073001.

(33) Ponce Ortiz, R.; Casado, J.; Hernández, V.; López Navarrete, J. T.; Viruela, P. M.; Ortí, E.; Takimiya, K.; Otsubo, T. On the Biradicaloid Nature of Long Quinoidal Oligothiophenes: Experimental Evidence Guided by Theoretical Studies. *Angew. Chem., Int. Ed.* **2007**, *46*, 9057−9061.

(34) Sun, K.; Xiao, Z.; Lu, S.; Zajaczkowski, W.; Pisula, W.; Hanssen, E.; White, J. M.; Williamson, R. M.; Subbiah, J.; Ouyang, J.; Holmes, A. B.; Wong, W. W. H.; Jones, D. J. A molecular nematic liquid

https://doi.org/10.1021/acsomega.1c04120
ACS Omega 2021, 6, 27305−27314

crystalline material for high-performance organic photovoltaics. *Nat. Commun.* **2015**, *6*, 6013.
(35) Li, H.; Wu, Q.; Zhou, R.; Shi, Y.; Yang, C.; Zhang, Y.; Zhang, J.; Zou, W.; Deng, D.; Lu, K.; Wei, Z. Liquid-Crystalline Small Molecules for Nonfullerene Solar Cells with High Fill Factors and Power Conversion Efficiencies. *Adv. Energy Mater.* **2019**, *9*, 1803175.
(36) Song, H.; Gao, Y.; Li, W.; Tian, H.; Yan, D.; Geng, Y.; Wang, F. Synthesis and characterization of diketopyrrolopyrrole-based conjugated molecules flanked by indenothiophene and benzoindenothiophene derivatives. *J. Mater. Chem. C* **2015**, *3*, 11135−11143.
(37) Wang, Y.; Guo, H.; Harbuzaru, A.; Uddin, M. A.; Arrechea-Marcos, I.; Ling, S.; Yu, J.; Tang, Y.; Sun, H.; López Navarrete, J. T.; Ortiz, R. P.; Woo, H. Y.; Guo, X. (Semi)ladder-Type Bithiophene Imide-Based All-Acceptor Semiconductors: Synthesis, Structure−Property Correlations, and Unipolar n-Type Transistor Performance. *J. Am. Chem. Soc.* **2018**, *140*, 6095−6108.
(38) Hestand, N. J.; Spano, F. C. Expanded Theory of H- and J-Molecular Aggregates: The Effects of Vibronic Coupling and Intermolecular Charge Transfer. *Chem. Rev.* **2018**, *118*, 7069−7163.
(39) Gao, R.; Wu, B.; Liang, Z.; Zhao, X.; Deng, Y.; Tian, H.; Geng, Y. Electronic properties modulation of tetraoxidothieno[3,2-b]-thiophene-based quinoidal compounds by terminal fluorination. *Mater. Chem. Front.* **2020**, *4*, 891−898.
(40) Sbargoud, K.; Mamada, M.; Marrot, J.; Tokito, S.; Yassar, A.; Frigoli, M. Diindeno[1,2-b:2′,1′-n]perylene: a closed shell related Chichibabin's hydrocarbon, the synthesis, molecular packing, electronic and charge transport properties. *Chem. Sci.* **2015**, *6*, 3402−3409.
(41) Vegiraju, S.; Lin, C.-Y.; Priyanka, P.; Huang, D.-Y.; Luo, X.-L.; Tsai, H.-C.; Hong, S.-H.; Yeh, C.-J.; Lien, W.-C.; Wang, C.-L.; Tung, S.-H.; Liu, C.-L.; Chen, M.-C.; Facchetti, A. Solution-Processed High-Performance Tetrathienothiophene-Based Small Molecular Blends for Ambipolar Charge Transport. *Adv. Funct. Mater.* **2018**, *28*, 1801025.
(42) Shen, T.; Zhou, H.; Xin, J.; Fan, Q.; Yang, Z.; Wang, J.; Mei, T.; Wang, X.; Wang, N.; Li, J. Controllable microstructure of polymer-small molecule blend thin films for high-performance organic field-effect transistors. *Appl. Surf. Sci.* **2019**, *498*, 143822.
(43) Smith, J.; Hamilton, R.; McCulloch, I.; Stingelin-Stutzmann, N.; Heeney, M.; Bradley, D. D. C.; Anthopoulos, T. D. Solution-processed organic transistors based on semiconducting blends. *J. Mater. Chem.* **2010**, *20*, 2562−2574.
(44) Panidi, J.; Paterson, A. F.; Khim, D.; Fei, Z.; Han, Y.; Tsetseris, L.; Vourlias, G.; Patsalas, P. A.; Heeney, M.; Anthopoulos, T. D. Remarkable Enhancement of the Hole Mobility in Several Organic Small-Molecules, Polymers, and Small-Molecule:Polymer Blend Transistors by Simple Admixing of the Lewis Acid p-Dopant B(C6F5)3. *Adv. Sci.* **2018**, *5*, 1700290.
(45) Chou, L.-H.; Na, Y.; Park, C.-H.; Park, M. S.; Osaka, I.; Kim, F. S.; Liu, C.-L. Semiconducting small molecule/polymer blends for organic transistors. *Polymer* **2020**, *191*, 122208.
(46) Hamilton, R.; Smith, J.; Ogier, S.; Heeney, M.; Anthony, J. E.; McCulloch, I.; Veres, J.; Bradley, D. D. C.; Anthopoulos, T. D. High-Performance Polymer-Small Molecule Blend Organic Transistors. *Adv. Mater.* **2009**, *21*, 1166−1171.
(47) Kang, M.; Hwang, H.; Park, W.-T.; Khim, D.; Yeo, J.-S.; Kim, Y.; Kim, Y.-J.; Noh, Y.-Y.; Kim, D.-Y. Ambipolar Small-Molecule:-Polymer Blend Semiconductors for Solution-Processable Organic Field-Effect Transistors. *ACS Appl. Mater. Interfaces* **2017**, *9*, 2686−2692.

https://doi.org/10.1021/acsomega.1c04120
ACS Omega 2021, 6, 27305−27314